Journal of the European Ceramic Society **12** (1993) 131–138

Influence of Bridging Interactions on the Lifetime Behaviour of Coarse-Grained Al_2O_3

T. Fett & D. Munz

Kernforschungszentrum Karlsruhe, Institut für Materialforschung II, Universität Karlsruhe, Institut für Zuverlässigkeit und Schadenskunde im Maschinenbau, Postfach 3640, D-7500 Karlsruhe 1, Germany

(Received 10 November 1992; revised version received 8 February 1993; accepted 15 March 1993)

Abstract

In the past R-curve effects in ceramic materials were investigated mainly with specimens containing artificial macrocracks. In this paper it is investigated how the bridging interactions in coarse-grained Al_2O_3 will influence the subcritical crack growth and lifetime behaviour of specimens with natural crack populations. Calculations using averaged stress intensity factors show the development of surface cracks until failure. As a consequence of bridging interactions and the occurrence of a threshold stress intensity factor in the v–K relation, deviations may occur from the expected straight line in the Weibull representation of lifetimes.

R-Kurveneffekte in Keramiken wurden bisher überwiegend an Proben mit künstlich eingebrachten Makrorissen studiert. In dieser Arbeit wird untersucht, wie die Rißuferwechselwirkungen in grobkörnigem Al_2O_3 das unterkritische Rißwachstum und damit die Lebensdauer von Proben mit natürlichen Rissen beeinflussen. Berechnungen auf der Basis gewichteter Spannungsintensitätsfaktoren zeigen, wie sich Oberflächenrisse vom Moment der Lastaufbringung bis zum Versagen entwickeln. Als Konsequenz der durch die Rißuferwechselwirkungen bedingten Brückenspannungen und des Auftretens eines Schwellenwertes in der v–K-Beziehung sind Abweichungen der Lebensdauerverteilungen von einer Weibull-Geraden zu erwarten.

Précédemment, les effets de courbe R ont été étudiées sur les matériaux céramiques au départ, principalement, d'échantillons contenant des fissures macroscopiques artificielles. Dans cet article, nous étudions comment les interactions de pontage dans des alumines à gros grains influencent la taille du défaut critique et la durée de vie d'échantillons présentant une population de fissues naturelles. Des calculs utilisant les facteurs d'intensité de contrainte moyens montrent le développement de fissures de surface jusqu'à la rupture. Comme conséquence des interactions de pontage et de la présence d'un seuil pour le facteur d'intensité de contrainte dans la relation v–K, des déviations peuvent apparaître à partir de la droite attendue dans la représentation de Weibull des durées de vie.

Notation

a	Crack depth
a_0	Crack size without bridging interactions
A	Factor in the power law for subcritical crack growth
$2c$	Crack width
$\mathbf{E}$	Complete elliptical integral of the second kind
F	Failure probability
$\mathbf{K}$	Complete elliptical integral of the first kind
K_I	Mode I stress intensity factor
K_{I0}	Stress intensity factor for the onset of stable crack extension
m	Weibull exponent
N	Exponent in the power law for subcritical crack growth
S	Crack surface
t	Time
W	Specimen thickness
Y	Geometric function
δ	Crack opening displacement
δ_0	Characteristic displacement parameter for the bridging stresses
σ	Stress
σ_0	Characteristic bridging stress
φ	Parametric angle

Journal of the European Ceramic Society 0955-2219/93/$6.00

Subscripts

appl	Applied
A,B	Characteristic locations of the semi-elliptical crack
bend	Bending
br	Bridging
r	Reference (e.g. reference stress intensity factor)
th	Threshold
tip	Value at the crack tip

1 Introduction

In coarse-grained alumina the crack growth resistance increases with increasing crack extension due to friction-like crack–border interactions in the wake of the advancing crack. This has consequences for the strength and also for subcritical crack growth behaviour. Since spontaneous failure in strength tests is affected by bridging stresses,[1,2] it must be expected that delayed failure due to subcritical crack growth will be influenced, too. This must be the case for alumina[3,4] as well as for zirconia.[5]

In a recent paper[6] lifetime results obtained under constant load were presented for coarse-grained alumina. In a Weibull plot non-linear behaviour was observed, which can be seen from Fig. 1. Such behaviour can be caused, in principle, by a specific flaw population. In this paper it will be shown that it can be related to the *R*-curve effect, too.

As a result of the crack–surface interactions, the stress intensity factor acting at the crack tip K_{Itip} deviates from the externally applied K_{Iappl}[7,8]

$$K_{\mathrm{Itip}} = K_{\mathrm{Iappl}} - K_{\mathrm{Ibr}} \tag{1}$$

where K_{Ibr} is the bridging stress intensity factor. This relation is the basis for understanding *R*-curve influences on lifetime behaviour. For its evaluation one needs the applied stress intensity factor caused by an externally applied load as well as the bridging stress intensity factor.

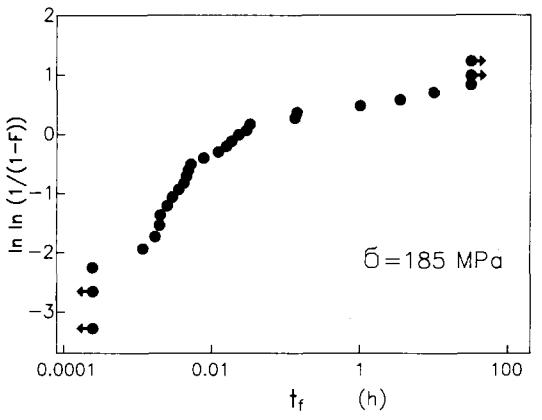

Fig. 1. Lifetimes measured in a static bending test at 20°C in air for coarse-grained Al_2O_3.

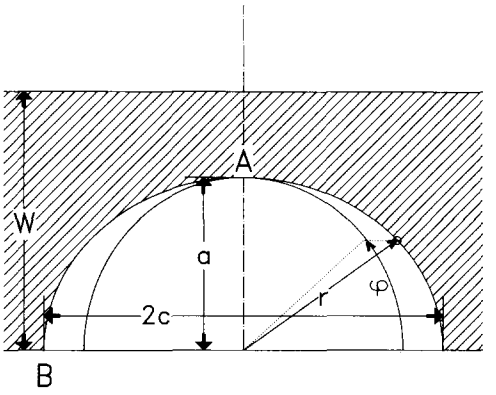

Fig. 2. Semi-elliptical surface crack in a ceramic specimen (not true scale).

2 Stress Intensity Factors

2.1 Applied stress intensity factor

The cracks in the surface region of ceramic materials caused by surface grinding which propagate under externally applied load are assumed to be semi-elliptical in shape. Different types of stress intensity factors are applicable to two-dimensional crack problems. One possibility is to use local stress intensity factors which vary along the crack front. Such stress intensity factors are available for simple load cases.

Besides that, averaged stress intensity factors are also often used in fracture mechanics.[9–11] These stress intensity factors are calculated for specific points along the crack front, e.g. for points A and B of a semi-elliptical surface crack (Fig. 2). They are obtained for a virtual crack extension as shown in Fig. 3 and described by

$$\Delta S_{\mathrm{A}} = \tfrac{1}{2}\pi c\,\Delta a \qquad \Delta S_{\mathrm{B}} = \tfrac{1}{2}\pi a\,\Delta c \tag{2}$$

Especially for the bending load case the resulting averaged stress intensity factors can be computed by

$$\bar{K}_{\mathrm{appl}_{\mathrm{A,B}}} = \sigma_{\mathrm{bend}}\,\bar{Y}_{\mathrm{A,B}}\sqrt{a} \tag{3}$$

with

$$\bar{Y}_{\mathrm{A}} = \left[\frac{4}{\pi}\int_0^{\pi/2} Y^2_{\mathrm{bend}}(\varphi)\sin^2\varphi\,\mathrm{d}\varphi\right]^{1/2} \tag{4.1}$$

$$\bar{Y}_{\mathrm{B}} = \left[\frac{4}{\pi}\int_0^{\pi/2} Y^2_{\mathrm{bend}}(\varphi)\cos^2\varphi\,\mathrm{d}\varphi\right]^{1/2} \tag{4.2}$$

For the numerical calculations the bending solution $Y_{\mathrm{bend}}(a/c,\ a/W,\ \varphi)$ given by Newman & Raju[12] is recommended. The geometrical quantities are illustrated in Fig. 2.

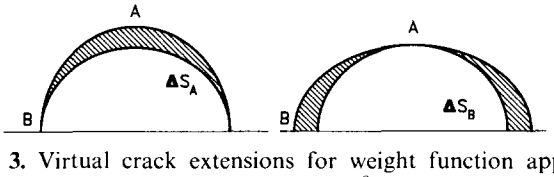

Fig. 3. Virtual crack extensions for weight function applications as proposed by Cruse & Besuner[9] (illustration restricted to one half of the embedded crack).

2.2 The bridging stress intensity factor

The friction-induced bridging stresses may be described by a number of relations between the bridging stresses σ_{br} and the crack opening displacement δ. Here an exponential relation is used as proposed in Ref. 13.

$$\sigma_{br} = \sigma_0 \exp(-\delta/\delta_0) \tag{5}$$

with a maximum stress σ_0 and a characteristic range δ_0. Bridging stress intensity factors are available only for some special crack types, for example edge cracks, penny-shaped embedded cracks and in an approximative solution also for embedded elliptical cracks.[2] It is assumed that the *R*-curve resulting for the embedded elliptical crack will also describe with sufficient accuracy the behaviour of semi-elliptical surface cracks.

An initially penny-shaped crack of radius a_0 is considered. Under an external load this crack may have propagated up to the actual dimensions of the two semi-axes a and c as illustrated in Fig. 4. Whilst the initial crack area is free from bridging stresses, bridging stresses are effective in the outer region (between the dashed and the solid lines).

The bridging stress intensity factor K_{Ibr} for elliptical embedded cracks was calculated applying the weight function method. According to Ref. 2, the results can be approximated by

$$\bar{K}_{br_{A,B}} = \sigma_0 \sqrt{a}\, \bar{Y}_{br_{A,B}} \tag{6}$$

with the geometric functions

$$\bar{Y}_{br_A} \simeq \frac{1-\exp[-C\sqrt{a/a_0 - a_0/a}]}{C\sqrt{a/a_0 - a_0/a}} \times \frac{4}{\pi \mathbf{E}(k)\bar{Y}_{r,A}} \int_0^{\pi} \left[\sin^2\varphi \sqrt{1-a_0^2/r^2} + \frac{1}{3}\left(\cos^2\varphi + \frac{1}{(c/a)^2-1}\frac{\mathbf{E}(k)-\mathbf{K}(k)}{\mathbf{E}(k)}\right) \times (1-a_0^2/r^2)^{3/2} \right] d\varphi \tag{7.1}$$

$$\bar{Y}_{br_B} \simeq \frac{1-\exp[-C\sqrt{a/a_0 - a_0/a}]}{C\sqrt{a/a_0 - a_0/a}} \times \frac{4}{\pi \mathbf{E}(k)\bar{Y}_{r,B}} \int_0^{\pi} \left[\cos^2\varphi \sqrt{1-a_0^2/r^2} - \frac{1}{3}\left(\cos^2\varphi + \frac{1}{(c/a)^2-1}\frac{\mathbf{E}(k)-\mathbf{K}(k)}{\mathbf{E}(k)}\right) \times (1-a_0^2/r^2)^{3/2} \right] d\varphi \tag{7.2}$$

where $\mathbf{K}(k)$ and $\mathbf{E}(k)$ are the complete elliptical integrals of the first and second kind with the modulus $k = \sqrt{1-a^2/c^2}$ and r defined in Fig. 2.

The reference stress intensity factors (subscript r)

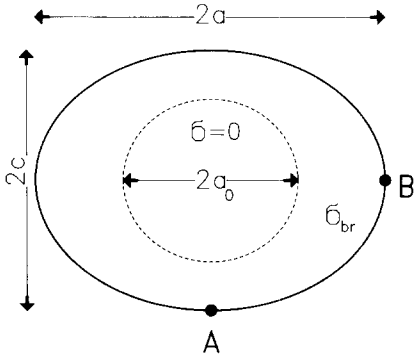

Fig. 4. Embedded elliptical crack developed from an initial circular crack of radius a_0.

are described by the geometric functions

$$\bar{Y}_{r,A} = \sqrt{\frac{4}{3\mathbf{E}(k)}\left(2 + \frac{1}{c^2/a^2-1}\frac{\mathbf{E}(k)-\mathbf{K}(k)}{\mathbf{E}(k)}\right)} \tag{8.1}$$

$$\bar{Y}_{r,B} = \sqrt{\frac{4}{3\mathbf{E}(k)}\left(1 - \frac{1}{c^2/a^2-1}\frac{\mathbf{E}(k)-\mathbf{K}(k)}{\mathbf{E}(k)}\right)} \tag{8.2}$$

C is defined as

$$C = \frac{4 \times 1{\cdot}141(1-\nu^2)K_{Itip}\sqrt{a_0}}{YE\pi\delta_0} \tag{9}$$

where $Y = 2/\sqrt{\pi}$, E = Young's modulus, ν = Poisson ratio.

The occurrence of K_{Itip} in the quantity C makes iterative solutions necessary. In the following expressions the bars on the averaged stress intensity factors and related geometric functions will be dropped.

3 Crack Propagation Under Constant Load

Surface cracks in ceramic materials caused by surface grinding are commonly assumed to be semi-circular in shape. During crack extension in bending a change of the crack shape must be expected. Therefore, bridging stress intensity factors for semi-elliptical surface cracks are also necessary. In the subsequent considerations the assumption will be made that bridging stress intensity factors for surface cracks can be approximated by the bridging stress intensity factors of embedded cracks with the same aspect ratio.

3.1 Material data and initial crack dimensions

For numerical computations the following material parameters were chosen according to a previous study,[2] where the strength behaviour of bending specimens with natural flaws has been adequately described

$$E = 3{\cdot}6 \times 10^5\ \text{MPa}$$
$$\nu = 0{\cdot}2$$
$$K_{I0} = 3\ \text{MPa}\sqrt{\text{m}}$$
$$\sigma_0 = 120\ \text{MPa}$$
$$\delta_0 = 1\ \mu\text{m}$$

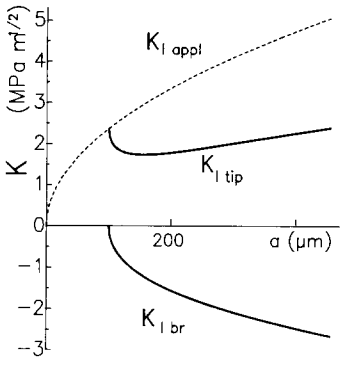

Fig. 5. Change of stress intensity factors during crack extension under constant load.

where K_{I0} = stress intensity factor for the onset of stable crack propagation. The crack sizes could be described by a two-parametric Weibull distribution

$$F(a_0) = \exp\left[-\left(\frac{a_{00}}{a_0}\right)^m\right] \tag{10}$$

with the Weibull parameters

$$a_{00} = 200\,\mu\text{m}$$
$$m = 2$$

All calculations are performed for a specimen thickness $W = 3{\cdot}5$ mm that was used also in the experimental lifetime tests. The specimen width is assumed to be large so that finite width correction is neither necessary for the bridging stress intensity factor nor for the externally applied stress intensity factor.

Whilst in strength tests crack propagation occurs with a constant crack tip stress intensity factor, namely $K_{I\text{tip}} = K_{I0}$, the value of $K_{I\text{tip}}$ must change with $K_{I\text{appl}}$ and $K_{I\text{br}}$ according to eqn (1) during subcritical crack growth in a test performed under static load. This behaviour is schematically explained in Fig. 5. The applied stress intensity factor $K_{I\text{appl}}$ (dashed curve) increases monotonically with crack extension. The bridging stress intensity factor is negative and also increases with crack extension. The sum of these two curves is the crack-tip stress intensity factor $K_{I\text{tip}}$, which first decreases significantly with increasing crack length, passes a minimum value and increases again.

Unfortunately, subcritical crack growth does not start in all cases at the initial crack size. This has to be considered especially for relatively high loads applied. Figure 6 illustrates the problem.

- In the case of a low applied stress σ_1 it holds that

$$K_{I\text{appl,A}},\ K_{I\text{appl,B}} < K_{I0}$$

and, consequently, the crack can propagate only by subcritical crack growth, starting from a_0, c_0.

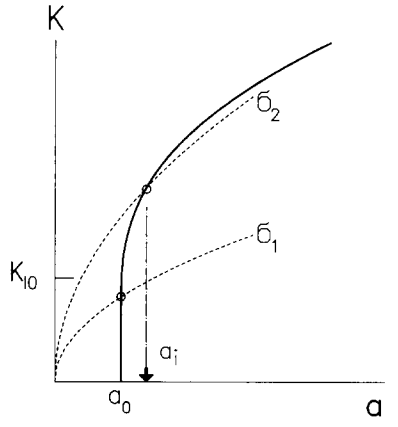

Fig. 6. Definition of initial crack size for a constant load test.

- In the case of a higher stress, $\sigma_2 > \sigma_1$, the crack will extend at the moment of load application up to a crack of dimensions $a' \geq a_0$, $c' \geq c_0$ which are given by the solution of the equations

$$\sigma_b Y_A(a'/c', a'/W)\sqrt{a'} - K_{I\text{br,A}}|_{\Delta a = a' - a_0} = K_{I0}$$
$$\sigma_b Y_B(a'/c', a'/W)\sqrt{a'} - K_{I\text{br,B}}|_{\Delta c = c' - c_0} = K_{I0} \tag{11}$$

In this case in eqn (9) the crack-tip stress intensity factor $K_{I\text{tip}}$ must be K_{I0}.

The crack growth relation describing subcritical crack growth rate, v, is assumed to be a power law

$$v = \frac{da}{dt} = \begin{cases} 0 & \text{for} \quad K_{I\text{tip}} < K_{I\text{th}} \\ A(K_{I\text{tip}})^N & \text{for} \quad K_{I\text{th}} < K_{I\text{tip}} < K_{I0} \\ \to\infty & \text{for} \quad K_{I\text{tip}} \geq K_{I0} \end{cases} \tag{12}$$

where $K_{I\text{th}}$ is the threshold stress intensity below which subcritical crack growth does not occur. From theoretical considerations a threshold stress intensity factor for thermally activated bond breaking must occur.[14,15]

3.2 Numerical procedure

Some details of the numerical evaluation of a static lifetime test will subsequently be explained for the special case of $K_{I\text{th}} = 0$. Immediately after load application the crack may have the dimensions a_0, $c_0 = a_0$ (case $\sigma = \sigma_1$ in Fig. 6).

Step 1: The stress intensity factors for this situation are

$$K_{I\text{appl A,B,0}} \quad \text{eqn (3)}$$
$$K_{I\text{br A,B,0}} = 0 \quad \text{eqns (6)–(9)}$$
$$K_{I\text{tip A,B,0}} = K_{I\text{appl A,B,0}} \quad \text{eqn (1)}$$

A crack size increment $da = \lambda a_0$, $\lambda \ll 1$ is chosen. The related crack increment dc_0 results from eqn (12) as

$$dc_0 = (K_{I\text{tip B,0}}/K_{I\text{tip A,0}})^N\, da \tag{13}$$

and the time increment needed for the crack extension da is

$$dt_0 = \frac{da}{AK^N_{I\,tip\,A,0}}$$

and the new crack dimensions are $a_1 = a_0 + da$; $c_1 = c_0 + dc_0$.

Step 2: The stress intensity factors for the extended crack are

$$K_{I\,appl\,A,B,1}$$
$$K_{I\,br\,A,B,1} = f(K_{I\,tip})$$
$$K_{I\,tip\,A,B,1} = K_{I\,appl\,A,B,1} - K_{I\,br\,A,B,1}$$

The next crack increments are

$$da$$
$$dc_1 = (K_{I\,tip\,B,1}/K_{I\,tip\,A,1})^N da$$

and the time increment becomes

$$dt_1 = \frac{da}{AK^N_{I\,tip\,A,1}}$$

$$t_1 = t_0 + dt_1$$

It should be noted that $K_{I\,br}$ depends on the crack-tip stress intensity factor $K_{I\,tip}$. There are several possibilities to determine $K_{I\,br}$ and $K_{I\,tip}$. The simplest ones are:

- Replacing the unknown value $K_{I\,tip}$ in eqn (9) by the value obtained in the preceding step, i.e.

  $$K_{I\,br\,A,B,n} = f(K_{I\,tip\,A,B,n-1})$$

  This is recommended above all for very small values of λ.
- The stress intensity factors $K_{I\,br}$, $K_{I\,tip}$ can be obtained from the solution of the implicit equation

  $$K_{I\,appl} - K_{I\,tip} - K_{I\,br}(K_{I\,tip}) = 0$$

  which can be found for each step by a zero-routine.

These steps are repeated until $K_{I\,tip} = K_{I0}$ and $dK_{I\,tip} > 0$ is fulfilled. The lifetime is given as the sum of all time increments.

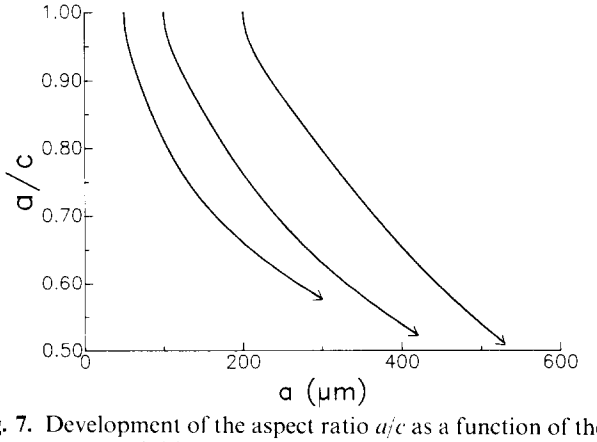

Fig. 7. Development of the aspect ratio a/c as a function of the initial crack size a_0 ($N = 30$).

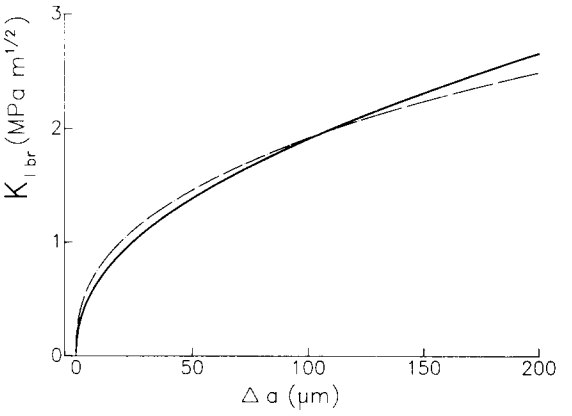

Fig. 8. R-Curves for the two points A (——) and B (– · –) computed with $a_0 = 200\,\mu m$, $\sigma_{bend} = 185$ MPa, $N = 30$.

In the case of $\sigma = \sigma_2$ the initially stable crack development is described by the eqn (11). This system of equations yields the crack dimensions a, c from which subcritical crack growth starts. The further computation is identical with that for $\sigma = \sigma_1$.

3.3 Numerical results

In Fig. 7 the development of the crack shape during a static bending test with 185 MPa bending stress is shown for initial crack sizes of $a_0 = 50$, 100 and 200 μm. The principal shape of the curves is identical with that of stable crack extension occurring in bending strength tests.

The related R-curves are shown in Fig. 8 for the crack with $a_0 = 200\,\mu m$. The R-curve for point A is plotted as a solid line and the R-curve for the surface point B as a dashed line. Both curves are nearly identical. Figure 9 represents the lifetime t as a function of the externally applied bending stress σ_{bend} for a crack of $a_0 = 200\,\mu m$ and a subcritical crack growth exponent $N = 30$. Whilst for a material without an R-curve effect a straight line with slope $-1/N$ has to be expected (dashed line) the curve (solid line) deviates from a straight line in the case of an R-curve effect due to bridging stresses and the steepness of the curve is significantly lower.

This is in agreement with earlier results obtained by the authors.[4,13] The existence of a threshold

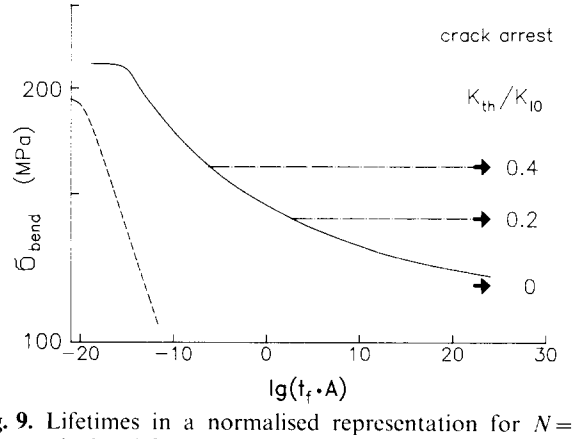

Fig. 9. Lifetimes in a normalised representation for $N = 30$, calculated for a crack of initial size $a_0 = 200\,\mu m$.

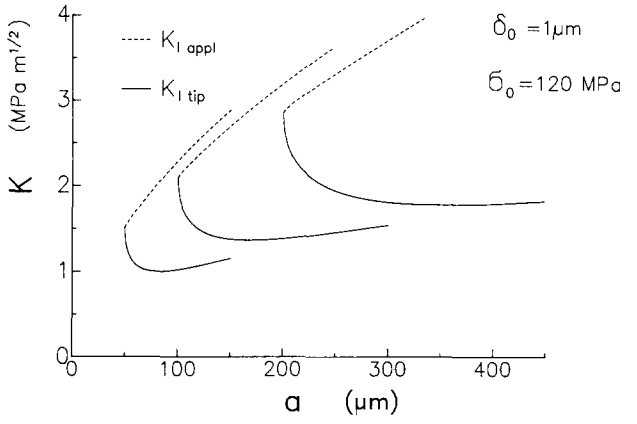

Fig. 10. Influence of the initial crack size a_0 on the applied and crack-tip stress intensity factors.

stress intensity factor $K_{I\,th}$ affects the limit stress value below which crack arrest occurs. The development of the crack-tip stress intensity factor $K_{I\,tip}$ is illustrated in Fig. 10 for several initial crack sizes. For lifetimes especially the regions around the minimum values of $K_{I\,tip}$ (named $K_{I\,tip,min}$) are of the most importance, since crack extension here takes the main part of the whole lifetime. The interdependency of minimum crack-tip stress intensity factor and initial crack size is plotted in Fig. 11. If a threshold stress intensity factor $K_{I\,th} > 0$ exists, all lifetime tests with $K_{I\,tip,min} \leq K_{I\,th}$ will result in an infinite lifetime, since crack arrest must occur.

Finally, the distribution of the lifetimes is shown in Fig. 12 for the crack size distribution described by eqn (10) and different $K_{I\,th}$ values selected. Figure 12(a) represents the results for $N = 20$ and Fig. 12(b) for $N = 30$. The solid lines, which describe the lifetime behaviour in the absence of a threshold stress intensity factor, have the same shape as the fitted strength curve in Ref. 2. The influence of a threshold value $K_{I\,th}$ leads to a stronger non-linearity of the lifetime distribution. A sufficient description

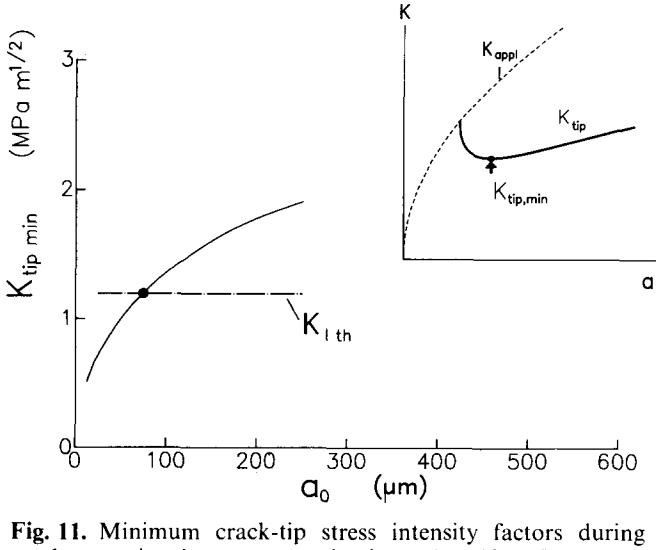

Fig. 11. Minimum crack-tip stress intensity factors during crack extension in a constant load test ($\sigma = 185$ MPa) (crack arrest situation for $K_{I\,th} = 0{\cdot}4K_{I0}$ indicated by solid circle).

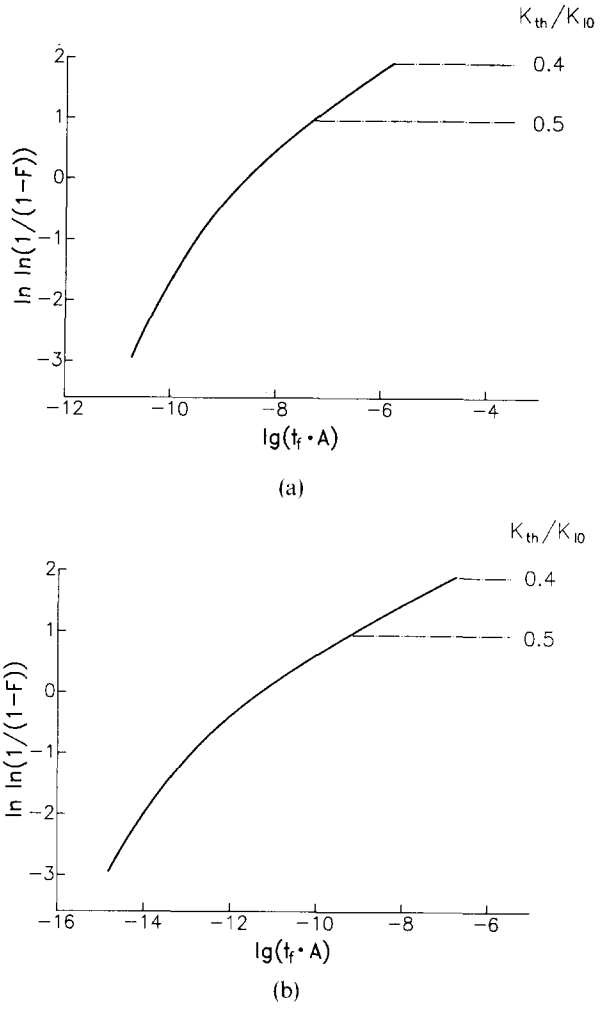

Fig. 12. Weibull distribution of lifetimes under $\sigma_{bend} = 185$ MPa, computed for (a) $N = 20$ and (b) for $N = 30$ (dash dotted lines: influence of a threshold stress intensity factor).

of the measured lifetime by the calculations can be found for

$$N = 20$$
$$K_{I\,th}/K_{I0} = 0{\cdot}5$$
$$\log A = -10{\cdot}8 \ (A \text{ in MPa m s}) \qquad (14)$$

With these data the computed lifetime distribution is plotted in Fig. 13 together with the measured data of Fig. 1. The only deviation worth mentioning is that

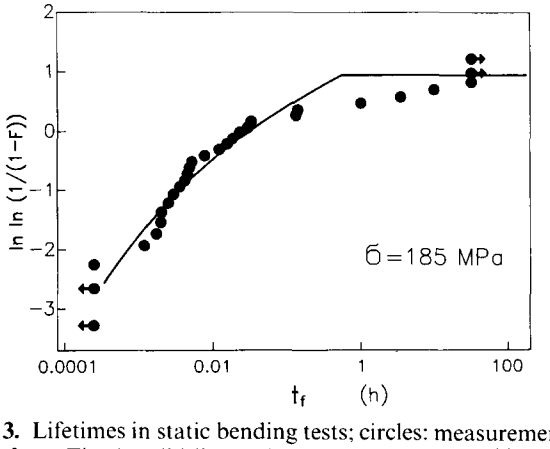

Fig. 13. Lifetimes in static bending tests; circles: measurements from Fig. 1, solid line: calculated with data set.[14]

Table 1. Comparison of subcritical crack growth with bridging parameters

Test	*Crack type*	*Reference*	*N*	*log(A)* (*A in MPa m s*)	σ_0 (*MPa*)	δ_0 (μm)
Static tests	Microcracks	This study	20	−10·8	120	1
Static tests	Macrocracks	13	25	−15·9	46·4	0·95

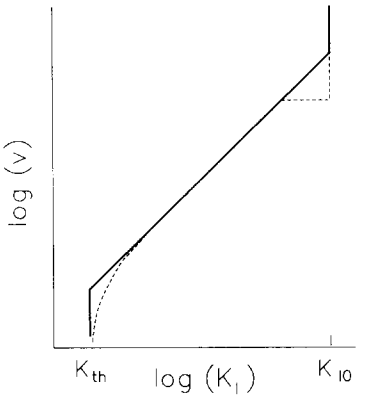

Fig. 14. Threshold behaviour; solid lines: eqn (12), dashed curve: realistic behaviour (stress intensity factors in terms of $K_{I\,tip}$).

the threshold effect does not begin as abruptly as calculated. Also this effect can be understood from the v–K behaviour plotted in Fig. 14. The solid lines represent eqn (12). It can be shown theoretically[14,15] that the threshold effect is asymptotically reached and the transition from $v > 0$ to $v \to 0$ is smoother than given by eqn (12). This more realistic behaviour is illustrated by the dashed curve. Having this in mind, the deviations in Fig. 13 are self-explanatory.

The bridging parameters and the parameters of subcritical crack extension are compared in Table 1 with parameters obtained from static tests with specimens containing macrocracks. The bridging stresses obtained from the tests with macrocracks are lower than those obtained in the tests with microcracks. The parameter N is similar; however, the parameter A is considerably lower for the macrocracks.

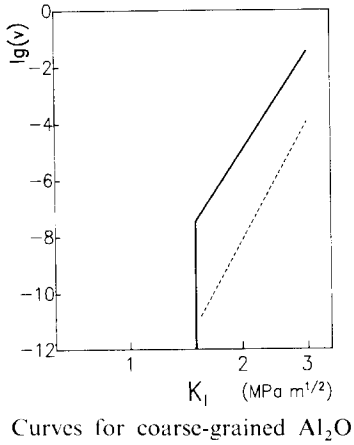

Fig. 15. v–K_I Curves for coarse-grained Al_2O_3; solid curve: obtained from lifetime measurements; dashed curve: macrocrack result from Ref. 13 (stress intensity factors in terms of $K_{I\,tip}$).

In Fig. 15 the v–K_I curve obtained from macrocrack measurements[13] is plotted as a dashed line together with the microcrack relation proposed in this investigation (solid curve). The subcritical crack growth rates for the microcracks are significantly lower than the crack velocities obtained with macrocracks.

4 Discussion

The evaluation of the lifetime results shows that it is possible to explain the non-linear Weibull plot by the R-curve effect. The curves in Fig. 13 of the lifetime distribution and in Fig. 15 of the da/dt–K_I relations have been obtained from the bridging stress parameters σ_0 and δ_0 evaluated from the strength distribution. The freely selected parameters are N, A and K_{I0}.

The large discrepancy in the crack growth rate between microcracks and macrocracks can be reduced if lower values of σ_0 are applied. From Fig. 16 it can be seen that a reduction in σ_0 from 120 MPa to 100 MPa still leads to a reasonably good description of scatter in lifetime. The corresponding threshold value is 1·75 MPa$\sqrt{\text{m}}$. The corresponding growth rate parameters are $N = 20$, $\log A = -12{\cdot}8$, leading to a better agreement with the macrocrack behaviour, as can be seen from Fig. 17. However, the crack growth rate is still higher. Therefore, under the assumption made it continues to apply that the bridging stresses for microcracks are larger than for macrocracks and that the crack growth rate for the same crack-tip stress intensity factor $K_{I\,tip}$ is higher

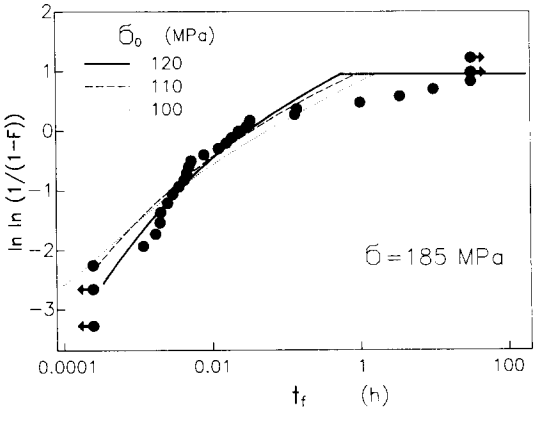

Fig. 16. Influence of the chosen value σ_0 on the lifetime distribution.

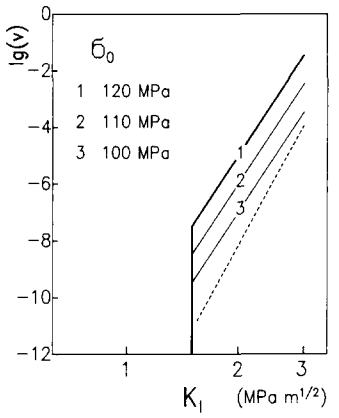

Fig. 17. Influence of the chosen value σ_0 on the v–K_I curves (stress intensity factors in terms of $K_{I\,tip}$).

for the microcracks. A further decrease in σ_0 for the microcracks would yield a lifetime distribution not agreeing with the experimental results.

It cannot be excluded that the assumptions made influence the result. These assumptions are: Weibull distribution without R-curve effects, application of averaged instead of local stress intensity factors, approximation of R-curves of surface cracks by R-curves of embedded cracks.

Considering all these assumptions, nevertheless, the cautious conclusion may be drawn that the da/dt–$K_{I\,tip}$ relation of microcracks and macrocracks deviate from each other. There may be different reasons for this effect. Generally, the linear elastic relations are not fully correct for small cracks as can be seen from strength tests. It is also possible that the stress intensity factor of a real flaw/crack configuration, e.g. a pore with a circumferential crack, deviates from that of a flat crack. Also the experimental finding of Steinbrech & Schmenkel[16] that in stable crack growth tests small cracks can grow under significantly lower applied stress intensity factors than are necessary for macrocracks may be valid for subcritical growth, too.

5 Summary

In this paper it has been illustrated how the R-curve effects caused by bridging interactions of the crack surfaces will influence the lifetimes in static bending tests for specimens with natural crack populations.

With the parameters σ_0, δ_0, K_{I0} the strength and lifetime behaviour including scatter can be described completely.

Calculations using averaged stress intensity factors show the development of surface cracks under conditions of subcritical crack growth in a lifetime test. It can easily be concluded that the crack shape during crack extension in static bending tests is not constant.

Experimental lifetimes are compared with results calculated on the basis of bridging parameters obtained from an evaluation of bending strength. Considering a threshold stress intensity factor in the power law representation of subcritical crack growth, the measured lifetime distribution can be interpreted. Deviations were found between the microcrack v–K_I-relation and the macrocrack results given in Ref. 13.

References

1. Bennison, S. J. & Lawn, B. R., Flaw tolerance in ceramics with rising crack resistance characteristics. *J. Mater. Sci.*, **24** (1989) 3169–75.
2. Fett, T. & Munz, D., Submitted to *Comm. Amer. Ceram. Soc.*
3. Fett, T. & Munz, D., Subcritical crack growth of macro- and microcracks in ceramics. *Fract. Mech. Ceram.*, **9** (1992) 219–33.
4. Fett, T. & Munz, D., Influence of R-curve effects on lifetimes for specimens with natural cracks. *Proc. of the Conf. on Fracture Processes in Brittle Disordered Materials.* Noordwijk, The Netherlands, 19–21 June 1991, Vol. 1, pp. 365–74.
5. Proß, J., Unterkritisches Rißwachstum in gefügeverstärkten Keramiken. Thesis, University of Stuttgart, 1992.
6. Fett, T. & Munz, D., Static and cyclic fatigue of ceramic materials. In *Ceramics Today—Tomorrow's Ceramics*, ed. P. Vincezini. Elsevier Science Publishers BV, 1991, pp. 1827–35.
7. Lawn, B. R., Physics of fracture. *J. Amer. Ceram. Soc.*, **66** (1983) 83–91.
8. Mai, Y. & Lawn, B. R., Crack-interface grain bridging as a fracture resistance mechanism in ceramics: II. Theoretical fracture mechanics model. *J. Amer. Ceram. Soc.*, **70** (1987) 289.
9. Cruse, T. A. & Besuner, P. M., *J. Aircraft*, **12** (1975) 369–75.
10. Mattheck, C., Morawietz, P. & Munz, D., Stress intensity factor at the surface and at the deepest point of a semi-elliptical surface crack in plates under stress gradients. *Int. J. Fract.*, **23** (1983) 201–12.
11. Fett, T., Mattheck, C. & Munz, D., Approximate weight functions for 2D and 3D problems. *J. Engng Analysis*, **6** (1989) 48–62.
12. Newman, J. C. & Raju, I. S., An empirical stress-intensity factor equation for the surface crack. *Engng Fract. Mech.*, **15** (1981) 185–92.
13. Fett, T. & Munz, D., Evaluation of R-curves in ceramic materials based on bridging interactions. KfK-Report, 4940, Kernforschungszentrum Karlsruhe, 1991.
14. Fuller, E. R. & Thomson, R. M., Lattice theories of fracture. In *Fracture Mechanics of Ceramics*, IV. Plenum Press, 1978, pp. 507–48.
15. Fett, T., A fracture-mechanical theory of subcritical crack growth in ceramics. *Int. J. Fract.*, **54** (1992) 117–30.
16. Steinbrech, R. & Schmenkel, O., Crack resistance curves for surface cracks in alumina. *Comm. J. Amer. Ceram. Soc.*, **72** (1988) C271.